Photochemical & Photobiological Sciences

Accepted Manuscript

This article can be cited before page numbers have been issued, to do this please use: D. A. Lukyanov, L. D. Funt, A. S. Konev, A. Povolotskiy, A. A. Vereshchagin, O. Levin and A. F. Khlebnikov, *Photochem. Photobiol. Sci.*, 2019, DOI: 10.1039/C9PP00206E.

ROYAL SOCIETY OF CHEMISTRY

rsc.li/pps

View Article Online
DOI: 10.1039/C9PP00206E

Journal Name

COMMUNICATION

Novel homogeneous photocatalyst for oxygen to hydrogen peroxide reduction in aqueous media

Received 00th January 20xx,
Accepted 00th January 20xx

DOI: 10.1039/x0xx00000x

www.rsc.org/

Daniil A. Lukyanov,[a] Liya D. Funt,[a] Alexander S. Konev,*[a] Alexey V. Povolotskiy,[a] Anatoly A. Vereshchagin,[a] Oleg V. Levin[a] and Alexander F. Khlebnikov [a]

An isoquinolinium-pyrrole donor-acceptor dyad was found to exhibit photocatalytic activity in oxygen-to-peroxide photoreduction with oxalate as a sacrificial electron donor. The concentration of hydrogen peroxide was shown to reach plateau of 0.57 mM. The screening of related pyridinium-pyrrole dyads showed the importance of isoquinoline moiety in securing the photocatalytic activity.

Environmental conservation fosters the search for energy sources alternative to fossil fuel, the energy of sun irradiation being most appealing among them.[1–3] The natural way for solar energy conversion, the photosynthesis, has low quantum and mass efficiency. The charge separation state of the photosystem II accumulates only 0.5 eV from the total photon energy due to multiple energy losses during the cascade charge separation.[1,4] To increase the efficiency of solar energy harvesting, extensive efforts have been devoted to the development of artificial photocatalytic systems, which accumulate the power of light in the energy of chemical bonds.[1,5–7]

Photoreduction of oxygen to hydrogen peroxide[5] is an example of this approach, as hydrogen peroxide is one of the most powerful and cheap oxidants used in chemical and pharmaceutical industry. Oxidation processes involving H_2O_2 are known to be selective, clean and green.[8] In addition, H_2O_2 is believed to be useful green fuel able to produce electric power in fuel electrochemical cells.[9,10] At present, hydrogen peroxide is mainly produced by the costly, energy-consuming and hazardous anthraquinone process,[11] so the development of photocatalytic processes for H_2O_2 synthesis would have a positive environmental impact.

In the pioneering works in the field of photocatalysis, mainly inorganic materials, such as TiO_2[12,13] and ZnO,[14,15] have been utilized as photocatalysts. However, poor absorption of visible light by such inorganic photocatalysts has limited their utilization for light harvesting. Dye sensibilization[16] or utilization of nanoparticles[17,18] can increase the light absorption by such systems. Alternatively, application of organic molecules as photocatalysts based on acridinium[19–22] or quinolinium[23–28] carcasses allows to enhance catalyst efficiency by performing the reaction in the homogenous mode in addition to the increased light absorption. In particular, photocatalytic reduction of O_2 to H_2O_2 using a mesitylacridinium donor-acceptor dyad **I** (Fig. 1) as a photocatalyst has been reported by Fukuzumi et al.[21]

Environmentally friendly conversion of O_2 to H_2O_2 requires strong and "green" reductant. A perfect candidate seems to be an oxalate ion due to its high reductive power (E_0 = 0.475 V *vs.* NHE), abundance in natural sources and CO_2 as the only by-product (eq. 1),[26–28] the last factor being the advantage over conventional sacrificial electron donors such as aromatic[22,23] and polyaromatic hydrocarbons,[20,21] alcohols,[19,29] phenols,[23] and amines.[30]

$$C_2O_4^{2-} + O_2 + 2H^+ = 2CO_2 + H_2O_2 \quad \text{(eq. 1)}$$

In our work, we explore pyrrolo-isoquinolinium and pyrrolo-pyridinium dyads **IIa-d**[31] and **IIIa-d**[32] as a novel kind of compact donor-acceptor system potentially able to photocatalyze the process of O_2 to H_2O_2 reduction with oxalate ions and compare their performance to mesitylacridinium **I**.

A series of experiments was performed in order to evaluate the photocatalytic activity of compounds **IIa-d** and **IIIa-d** (Fig. 1) for O_2 reduction with oxalate as a sacrificial donor. A portion of each compound was dissolved in 8 mL of sodium oxalate buffer (*p*H 4.5), the solutions obtained were irradiated by LED light source with λ_{max} = 415 nm and light emitting power of *ca.* 0.33 W while being maintained at 8 °C with air bubbling. After 3 h of continuous irradiation, a sample of solution was collected and the hydrogen peroxide content was evaluated immediately using photometric titanyl oxalate technique[33] and iodometric technique[34] to secure confident detection of H_2O_2.

Screening of the series **IIa-d** showed that only the pyrrole-isoquinolinium dyad **IIa** possesses discernible photocatalytic activity. None of pyridinium-containing analogues shows any

[a] *Institute of Chemistry, Saint Petersburg University, 7/9 Universitetskaya nab., St. Petersburg 199034, Russia, E-mail: a.konev@spbu.ru, a.khlebnikov@spbu.ru.*
Electronic Supplementary Information (ESI) available: calibration curve for titanyl oxalate photometric analysis, UV-Vis spectra of compounds I-III, other data on electrochemical and photophysical study of IIa. See DOI: 10.1039/x0xx00000x

View Article Online
DOI: 10.1039/C9PP00206E

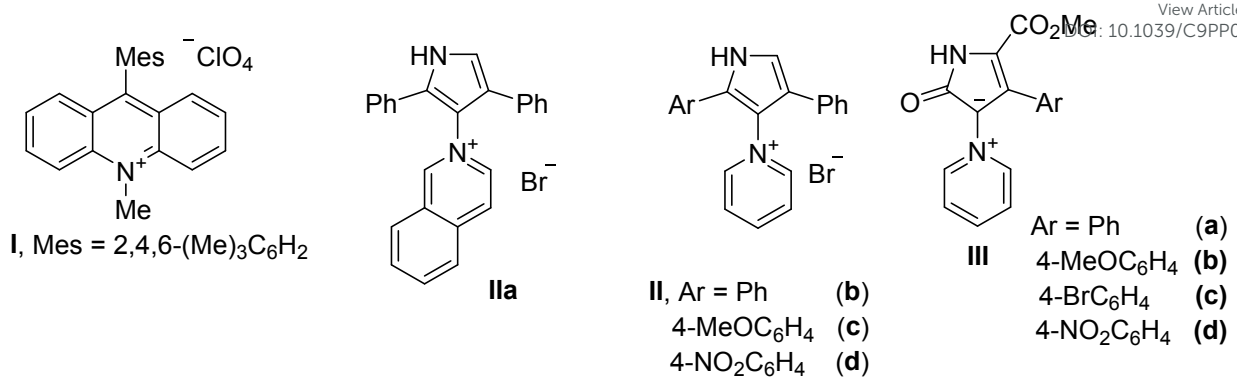

Figure 1. Structures of compounds **I**, **IIa-d**, **IIIa-d**. Donor fragments are colored in blue, acceptor fragments in red.

photocatalytic activity. On the other hand, *N*-methylisoquinolinium tetrafluoroborate has zero absorption above 360 nm (SI, Fig. SI3), and the isoquinolinium fragment by itself cannot thus account for the observed activity of **IIa**. This lead us to conclusion that combination of pyrrole and isoquinolinium fragments is necessary to provide the observed photocatalytic reduction of O_2 to hydrogen peroxide.

A series of control experiments was performed to establish the necessity of each factor for H_2O_2 generation: the catalyst, the oxygen and the light. None of the control experiments (irradiation without the catalyst, without the irradiation and the irradiation under Ar atmosphere) produced any amount of H_2O_2, confirming it is the photocatalytic reduction of O_2 with direct involvement of **IIa** as a catalyst.

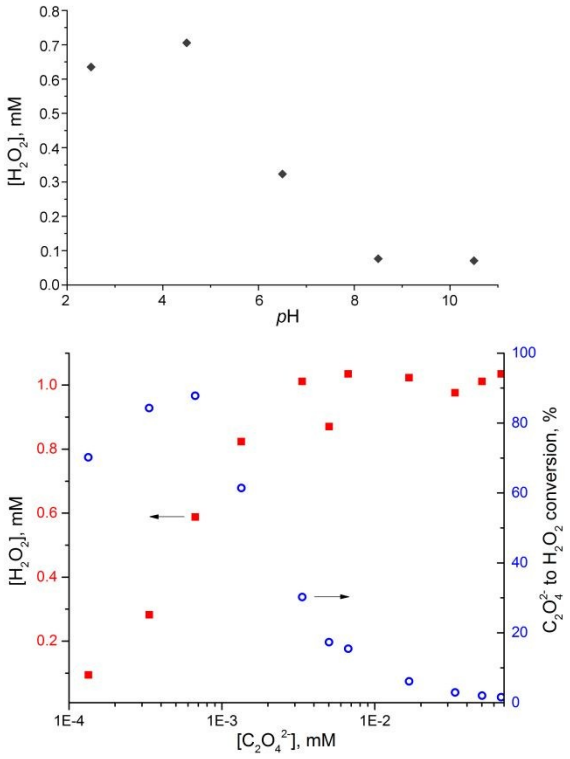

Figure 2. The *p*H (top, 67 mM oxalate solution) and $[C_2O_4^{2-}]$ (bottom, red squares, *p*H 4.5) dependence of concentration of H_2O_2 in the reaction medium after 3h of irradiation (λ 415 nm) in the presence of compound **IIa**. (Air bubbling through the aqueous reaction medium at 8°C.) Blue circles show conversion of oxalate ions to H_2O_2.

In accord with the reaction equation, the production of H_2O_2 depended on both *p*H of the medium and concentration of oxalate ions. The *p*H screening showed that *p*H of 4.5 resulted in the highest production of H_2O_2 (Fig. 2) measured after 3h of the reaction. At this *p*H, the concentration of H_2O_2 produced in 3 h increased from 0.1 mM in 0.13 mM oxalate buffer to 1 mM in 7 mM oxalate buffer. Further increase of oxalate concentration did not affect the H_2O_2 accumulation rate (Fig. 2).

The time course of photocatalysis was recorded until the persistent concentration of hydrogen peroxide was reached. An array of 8 LEDs with overall light emitting power of ca. 2.64 W was used for these reactions to irradiate 0.1 mM solutions of catalysts in oxalate buffer. In addition, each sample was examined for catalyst degradation by monitoring the absorbance of sample solution in near UV range. In order to compare these results with the performance of the known compound, the same experiment was carried out with 9-mesityl-10-methylacridinium perchlorate **I**, a benchmark compound for photocatalytic oxygen reduction.[21]

Both compounds **I** and **IIa** demonstrate asymptotic curve for hydrogen peroxide production, reaching plateau of ca. 0.4 mM and ca. 0.55 mM H_2O_2 concentration for catalysts **I** and **IIa** respectively (Fig. 3).

The stationary conditions of H_2O_2 production when the rate of formation is equal to the rate of decomposition might be one of the reasons for the asymptotic behavior of the process. However, hydrogen peroxide is known to be stable at temperatures below 14 °C.[14] Consistent with this, no decomposition of H_2O_2 was observed in the control experiment on irradiation of H_2O_2 solution with 415 nm LED in the oxalate buffer used in the experiments on photochemical generation of H_2O_2. Also, experiments on photogeneration of H_2O_2 in solutions with pre-added aliquot of H_2O_2 (0.4, 0.8, 1.3 and 3.1 mM) show continuous grow of H_2O_2 concentration. These results refute the hypothesis about reaching the stationary conditions of hydrogen peroxide formation.

View Article Online
DOI: 10.1039/C9PP00206E

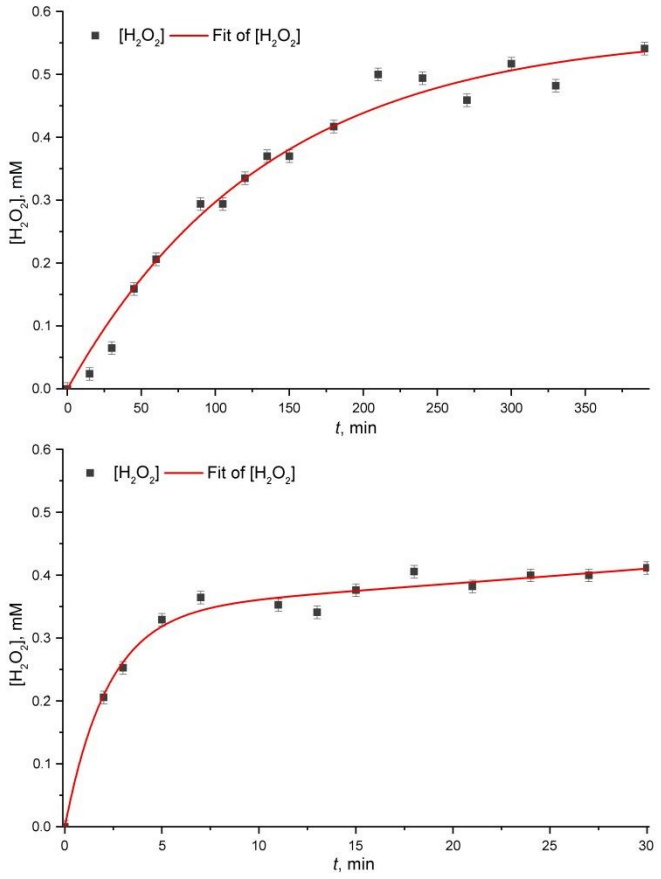

Figure 3. Time courses of H_2O_2 production for the experiments on irradiation (λ 415 nm, 8 °C) of air-bubbled oxalate aqueous solution (67 mM) using compounds **IIa** (*c* 0.1 mM) (top) and **I** (*c* 0.1 mM) (bottom). Fits of the experimental data are shown as solid lines.

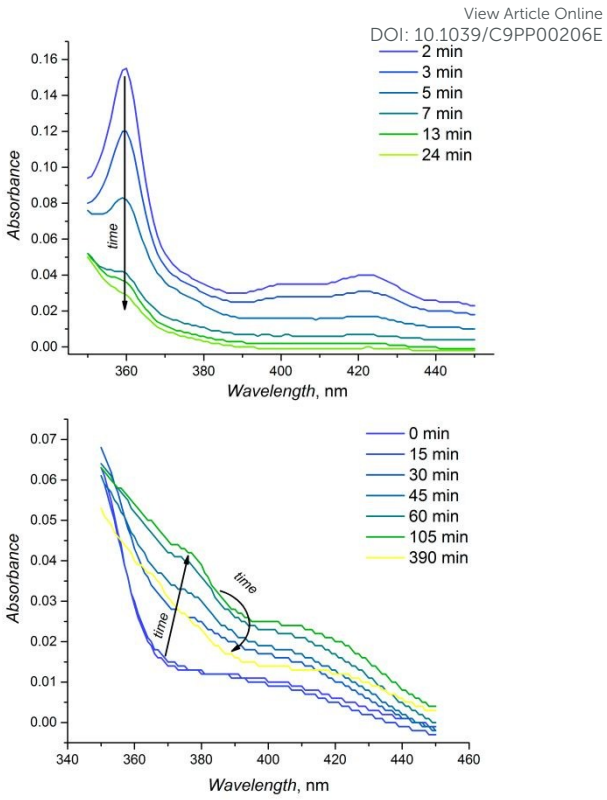

Figure 4. Time courses of catalyst degradation for the experiments using compounds **I** (*c* 0.1 mM)(top) and **IIa** (*c* 0.1 mM) (bottom).

An alternative cause for the asymptotic behavior might be the decomposition of the catalyst during the process. Indeed, almost complete depletion of the catalyst absorption bands was observed in the case of compound **I** within first 7 minutes of the reaction (Fig. 4, top). During twice the same time period, no changes were observed in the absorption spectrum of compound **IIa** (Fig. 4, bottom). However, longer exposition showed evolution of the absorption spectrum of the reaction medium, two new bands appearing at ca. 380 and ca. 420 nm. The new bands steadily grew during the first 100 min of the reaction. Subsequent overall fading of the absorption is most probably due to continuous degradation of the catalyst.

In view of the observed instability of the catalysts, the kinetics of the hydrogen peroxide production are best described by eq. 1, where the reduction of O_2 to H_2O_2 occurs with effective rate constant k_1 at the catalyst exponentially decaying with rate constant k_2. The effective rate constant k_1 takes into account that the concentrations of O_2 (permanent air flow) and H^+ (buffer solution) are constant.

$$\frac{d[H_2O_2]}{dt} = k_1 C^0_{cat} e^{-k_2 t} \qquad \text{(eq. 2)}$$

Solution of the differential equation 2 under boundary condition of $[H_2O_2] = 0$ at $t = 0$ gives the expression for the time evolution of the H_2O_2 concentration (eq. 3).

$$[H_2O_2] = \frac{k_1 C^0_{cat}}{k_2}\left(1 - e^{-k_2 t}\right) \qquad \text{(eq. 3)}$$

Fitting of the experimental data according to eq. 3 gives the effective rate constants for H_2O_2 generation, k_1, and catalyst decomposition, k_2, respectively for the processes catalyzed by the catalysts **I** and **IIa** (Table 1). Extrapolation of the H_2O_2 concentration to the infinity according to eq. 3 defines the asymptotic limit as $k_1C^0_{cat}/k_2$ to give 0.38 mM for compound **I** and 0.58 mM for compound **IIa**. So, despite the lower rate of H_2O_2 generation, compound **IIa** allows to reach the higher concentrations of H_2O_2 due to the higher stability of compound **IIa** under the experimental conditions.

To get insight on the mechanism of photocatalytic hydrogen peroxide formation by **IIa**, we performed a series of electrochemical and spectroscopic studies.

In cyclic voltammetry (CV) studies, compound **IIa** shows one reduction and one oxidation peak (Fig. 5). Exploring CV dependence on the potential sweep rate shows that the peak potentials stabilize at sweep rates of 50 mV/s at ca. 0 and –1.6 V (*vs.* TEMPOL/TEMPOL$^+$) for oxidation and reduction of **IIa** respectively. In view of the low dependence of the peak poten-

Table 1. The rate constants for the H_2O_2 photogeneration by use of catalysts **Ia** and **II**.

Catalyst	k_1, s^{-1}	k_2, s^{-1}	$k_1C^0_{cat}/k_2$, mM
I	$2.3(2)\cdot10^{-2}$	$6.1(6)\cdot10^{-3}$	0.38
IIa	$7.0(4)\cdot10^{-4}$	$1.2(1)\cdot10^{-4}$	0.58

tials on the potential sweep rates, the redox processes corresponding to these redox waves can be considered electrochemically reversible and can be used to estimate the formal electrode potentials. Taking the slowest (10 mV/s) potential sweep data for **IIa/IIa**$^+$ and **IIa/IIa**$^-$ redox couples corrected for 28 mV of polarization potential (–0.032 and –1.586 V respectively) as the closest assessments of the formal potentials, and considering formal potential E^o *vs.* SHE for TEMPO/TEMPO$^+$ reference couple of 0.750 V, one can estimate E^o *vs.* SHE values for **IIa/IIa**$^+$ and **IIa/IIa**$^-$ redox couples to comprise 0.718 and –0.836 V respectively. So, in view of the E^o values for other possible redox couples in the explored system, both reduction of **IIa** by oxalate ion and oxidation of **IIa** by molecular oxygen with formation of H_2O_2 are thermodynamically forbidden under standard conditions.

$O_2 + 2H^+ + 2e^- = H_2O_2$	E^o = 0.695 V
$H_2O_2 + 2H^+ + 2e^- = 2H_2O$	E^o = 1.76 V
$2CO_2 + 2H^+ + 2e^- = H_2C_2O_4$	E^o = –0.345 V
$Br_2 + 2e^- = 2Br^-$	E^o = 1.096 V
IIa$^+$ + e$^-$ = **IIa**	E^o = 0.718 V
IIa + e$^-$ = **IIa**$^-$	E^o = -0.836 V

However, these processes become thermodynamically allowed under non-standard conditions for certain ratios of the oxidized and reduced forms of **IIa** and H_2O_2 (Fig. 6). That means, a catalytic cycle involving transformations of compound **IIa** is thermodynamically allowed. Under these circumstances, the absence of the notable reaction in the dark shows that the role of light is to provide energy necessary to overcome the activation barrier endowing thus compound **IIa** with the properties of photocatalyst.

The UV-vis absorbance spectrum of compound **IIa** shows strong absorption in near UV region (λ_{max} 335 nm) with smaller shoulder at 400 nm extending to 490 nm (Fig. 7). Comparison to the model methyl isoquinolinium compound shows the 335 nm band to be due to absorption of the isoquinolinium fragment. Isoquinolinium compounds are reported to form intermolecular charge transfer complexes[35] or charge shift[36] exciplexes with aromatic hydrocarbons, showing charge transfer absorption band at 392–415 nm[35] or charge shift exciplex emission band at *ca.* 440–580 nm[36]. In view of these

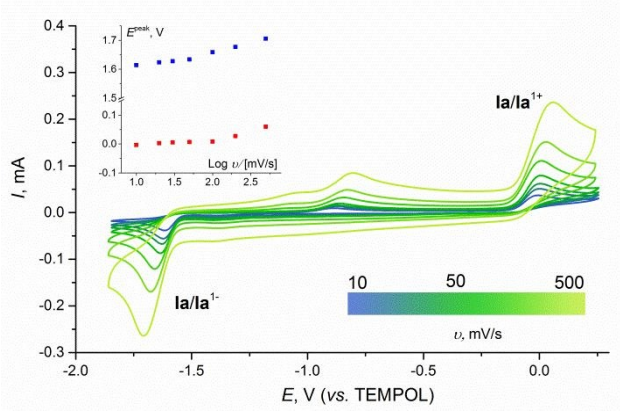

Figure 5. CVA of compound **IIa** (*c* 1 mM in DMF/$LiClO_4$ (0.1 M)) at variable potential sweep rate υ. Inset: dependence of oxidation (red dots) and reduction (blue dots) potential peaks on υ. Potentials are given vs. TEMPOL/TEMPOL$^+$ in the same medium.

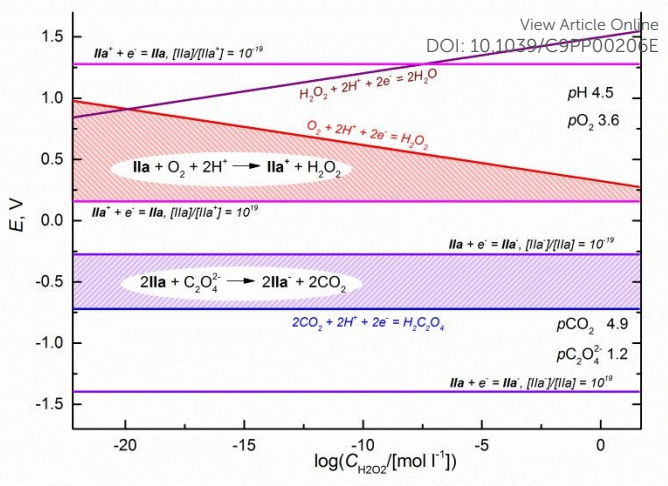

Figure 6. Electrode potential vs. H_2O_2 concentration diagram, *p*H 4.5, pO_2 3.6, pCO_2 4.9, $pC_2O_4^{2-}$ 1.2. Red area shows the range of [**IIa**]/[**IIa**$^+$] ratio corresponding to thermodynamically allowed oxidation of **IIa** to **IIa**$^+$ upon reduction of O_2 to H_2O_2. Violet area shows the range of [**IIa**$^-$]/[**IIa**] ratio corresponding to thermodynamically allowed reduction of **IIa** to **IIa**$^-$ upon oxidation of $C_2O_4^{2-}$ to CO_2.

data, we suppose the shoulder at 400 nm in the UV spectrum of **IIa** to be a charge transfer band due to the intramolecular charge transfer process from pyrrole to isoquinoline moiety.

TD DFT study of compound **IIa** testifies further to this hypothesis. According to DFT (B3LYP/6-31+G(d,p)) calculations, HOMO of **IIa** is localized on the diphenyl-pyrrole fragment, while LUMO is localized on the isoquinolinium moiety (Fig. 8). TD DFT modelling (PCM, water) predicts the lowest electronically excited state of **IIa** to have configuration HOMO^{1}LUMO^1 (>99% contribution of HOMO→LUMO transition to the formation of the state). The predicted energy of the state (2.57 eV/483 nm) and the low oscillator strength (0.0271) match well to the observed picture in the UV-Vis spectrum.

Emission spectra of compound **IIa** excited at the range 300–400 nm have peak at 445 nm with notable shoulder at 465 nm (Fig. 7). This two-peak pattern finds reflection in the excitation spectrum (450 nm emission), most probably being due to the vibronic structure of the CT absorption band (compound **IIa** has strong absorption at 1607, 1489 and 1393 cm^{-1}). At excitation with 390–400 nm light, the emission band is contaminated with the Raman scattering of water, but the two-peaks pattern remains at excitations with wavelengths shorter than 360 nm, where the Raman scattering band of water is shifted below 400 nm (Fig. 7, excitation at 340 nm). Interestingly, the emission at 350–400 nm (Fig. 7, bottom, red dot line), which corresponds to the fluorescence of the isoquinolinium moiety (Fig. 7, bottom, λ^{max} = 375 nm) is rather low. This is most probably due to the fluorescence quenching of the isoquinolinium fragment *via* the electron transfer from the pyrrole moiety, resulting in population of the CT state.

The lifetime of 450 nm CT emission band in **IIa** in the absence of oxalate ions and oxygen comprises 5.2 ns, giving the rate constant for radiative relaxation to the ground state k_{fl}=0.2·10^9 s^{-1}. Both the nanosecond time domain for the emission and the independence of the decay constant on the presence of oxygen testify to the singlet nature of the CT ex-

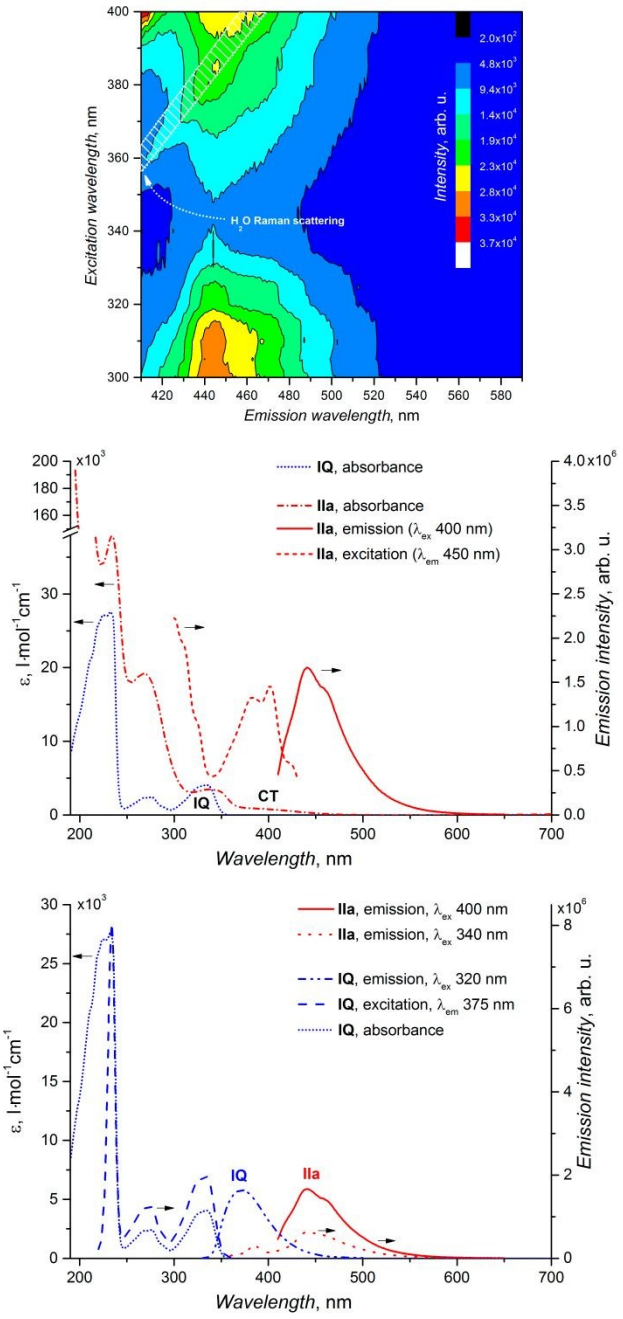

Figure 7. Top: 3D plot of excitation/emission spectra of compound **IIa**. Region covered with white pattern corresponds to the Raman scattering of water (3000–3700 cm^{-1} band). Middle and bottom: excitation (red short dash line, λ_{em} = 450 nm), emission (red solid line, λ_{ex} = 400 nm, red dot line, λ_{ex} = 340 nm) and absorption (red short dash dot line) spectra of compound **IIa** (c 0.01 mM (emission) and 0.22 mM (absorption) in water) *vs.* absorption (blue short dot line), excitation (blue dash line, λ_{em} = 375 nm) and emission (blue dash dot dot line, λ_{ex} = 320 nm) spectra of *N*-methylisoquinolinium tetrafluoroborate (**IQ**, *c* 0.1 mM (absorption) and 0.01 mM (emission) in water).

cited state. Additional conformation is the absence of the singlet oxygen fluorescence at 1270 nm for the studied system.

Unlike oxygen, oxalate ions demonstrate obvious quenching effect on the fluorescence of **IIa**. Both the fluorescence intensity (SI, Figs. SI15, SI16) and fluorescence lifetime (Fig. 9) depend strongly on the concentration of oxalate ions,

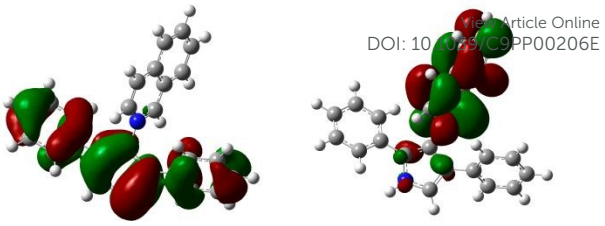

Figure 8. HOMO (left) and LUMO (right) of compound **IIa** according to DFT (B3LYP/6-31+G(d,p)) calculations.

implying involvement of a dynamic process to fluorescence quenching. In accord with this, Stern-Volmer plot for fluorescence intensity has non-linear character, while Stern-Volmer plot for fluorescence lifetime has linear character. Linear fit of the latter allowed to determine the rate constant of bimolecular fluorescence quenching with oxalate k_{red} to comprise $2.5 \cdot 10^9$ $M^{-1} \cdot sec^{-1}$ (Fig. 10).

Based on these data, the following mechanism for the photocatalytic activity of compound **IIa** for reduction of oxygen to hydrogen peroxide can be proposed (Fig. 11). Compound **IIa** is excited to a singlet electronically excited state upon irradiation with 420 nm light. The electronically excited state can undergo radiative relaxation to the ground state with constant rate of $0.2 \cdot 10^9$ s^{-1} or accept an electron from oxalate ion *via* electron transfer process with rate constant of $2.5 \cdot 10^9$ $M^{-1} \cdot sec^{-1}$. The reduced species of **IIa** is oxidized by molecular oxygen recovering **IIa** and leading to superoxide radical-anion, which eventually gives hydrogen peroxide.

In a set of compounds **IIIa-d**, the rise of absorbance at 400 nm was also noticed during photocatalytic experiment, and it was initially attributed to peroxotitanyl species. However, time courses of the abovementioned reactions showed a constant absorbance at 400 nm starting from *t* = 0 sec point. Further analysis of the samples by iodometric technique did not detect any H_2O_2 contained. Finally, addition of titanyl solution to the samples of compounds **IIIa-d** without irradiation caused an immediate rise of absorbance at 400 nm. These facts lead us to conclusion that the rise of absorbance at 400 nm observed in

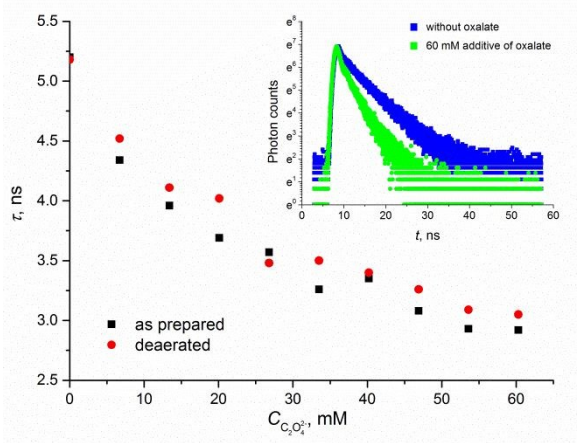

Figure 9. Dependence of fluorescence lifetime of compound **IIa** (aqueous solution, *c* 0.01 mM) on concentration of oxalate ions. Inset: kinetic trace for fluorescence at 465 nm (excitation at 390 nm).

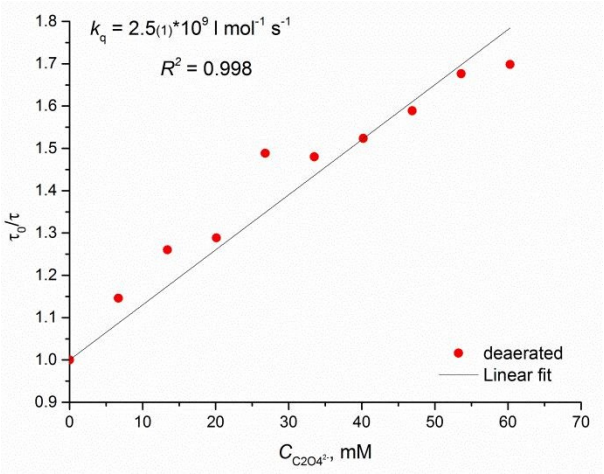

Figure 10. Stern-Volmer plot for fluorescence kinetics of compound **IIa** (water, *c* 0.01 mM) at variable concentrations of oxalate ions.

this case is caused by the formation of complexes of compounds **IIIa-d** with the titanium reagent used.

Conclusions

In a series of novel pyridinium- and isoquinolinium-pyrrole donor-acceptor dyads, isoquinolinium-pyrrole dyad **IIa** was shown to exhibit the photocatalytic activity in oxygen to peroxide reduction with catalytic performance comparable to the reference mesitylacridinium compound. While affording H_2O_2 concentration plateau similar to the reference compound (0.58 mM and 0.38 mM, respectively), dyad **IIa** shows better stability under the catalysis conditions. Most probable mechanism of the photocatalytic activity of dyad **IIa** includes electron transfer from oxalate ion to electronically excited molecule of the photocatalyst. Unlike isoquinolinium-pyrrole dyad, pyridinium-pyrrole dyads do not show photocatalytic activity.

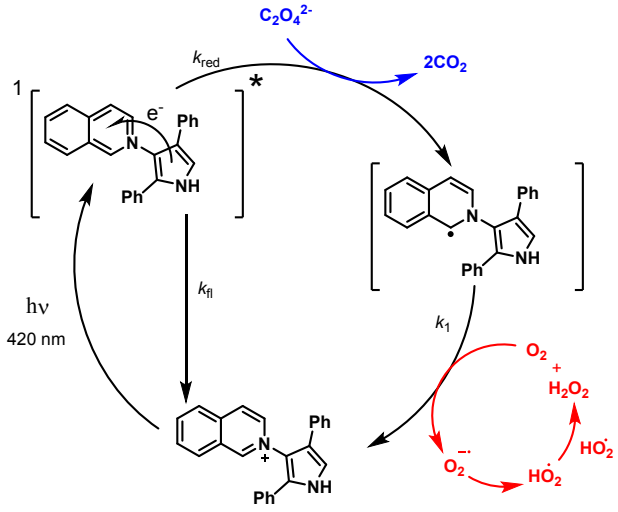

Figure 11. Proposed mechanism for reduction of O_2 to H_2O_2 with oxalate photocatalyzed by compound **IIa**.

Conflicts of interest

View Article Online
DOI: 10.1039/C9PP00206E

There are no conflicts of interest to declare.

Acknowledgements

This work was supported by Saint Petersburg State University (grant no. 12.40.1427.2017). Research was carried out with the support of the Research park of St. Petersburg State University Magnetic Resonance Research Center, Chemical Analysis and Materials Research Center, Center for Optical and Laser Materials Research, Educational Resource Center of Chemistry and Resource center "Computer center of Saint Petersburg State University".

Notes and references

‡ UV-Vis spectra were recorded on Shimadzu UV-1700 and UV-1800 spectrometers. Deionized water was obtained from Merck Millipore Simplicity purification system. Argon gas of 99,998% purity was used. Oxalate buffer with *p*H 4.5 was prepared by dissolution of 2 g of $H_2C_2O_4$ and 6 g of $Na_2C_2O_4$ in 1 L of deionized water. Solutions with *p*H of 2.5, 6.5, 8.5 and 10.5 were prepared by acidification of the initial buffer with 1 M H_2SO_4 or basification with 10% (w/w) NaOH until the required *p*H was reached. Inorganic chemicals were purchased from local suppliers. Compounds **I**,[35] **IIa-d**,[31] **IIIa-d**[32] were synthesized according to previously reported methods.

Photocatalytic experiments were performed in the self-made photoreactor. The irradiation source was made from HPL-H44TU1BA-V2 LED mounted on an efficient radiator and fed by LC-125/500-A AC/DC inverter. The reaction vessel was mounted in the way so that all 60° light cone lies within the transparent bottom of the vessel. The vessel was cooled by water jacket with 8° C water circulating inside and the mean temperature inside the reaction vessel was monitored by thermometer. Air bubbling was performed using an air pump connected through the syringe needle.

The H_2O_2 content was determined as follows: two aliquots (2 ml) of the reaction mixture were collected, 2.5 ml of H_2SO_4 (1:17 v/v) was added to each sample (**W** and **R**), then saturated $TiO(KC_2O_4)_2$ solution (2 ml) was added to the **W** sample, and finally both samples were diluted to 15 ml by deionized water. Then the UV spectra of **R** *vs* deionized water and **W** *vs* **R** were recorded immediately in the range of 350-450 nm. The absorbance at 400 nm was used to quantify the hydrogen peroxide content using the calibration plot recorded in the 4-80 μg sample content range.

Photoluminescence spectra and luminescence kinetic curves were measured on Horiba Fluorolog-3 spectrometer. The study of luminescent properties was carried out at a concentration of 0.01 mM, at which the optical density did not exceed 0.1 at the excitation wavelength for all samples. Luminescence kinetic curves were excited by LEDs with pulse duration of about 1 ns and measured with the Time-Correlated Single Photon Counting technic.

Geometry optimization of **IIa** was performed with the B3LYP density functional method and 6-31+G(d,p) basis set with PCM solvation model for water. Stationary point on the potential-energy surface was characterized by evaluating the Hessian

eigenvalues. Calculations of the excited states were performed using TD DFT method at the same level of theory.

1 I. McConnell, G. Li and G. W. Brudvig, Energy Conversion in Natural and Artificial Photosynthesis. *Chem. Biol.* 2010, **17**, 434–447.
2 C. F. Shih, T. Zhang, J. Li and C. Bai, Powering the Future with Liquid Sunshine. *Joule* 2018, **2**, 1925–1949.
3 Y. Lee, C. Park, N. Balaji, Y.-J. Lee and V. A. Dao, High-efficiency Silicon Solar Cells: A Review. *Isr. J. Chem.* 2015, **55**, 1050–1063.
4 K. Satoh, Isolation and Properties of the Photosystem II Reaction Center A2, in *Photosynthetic Reaction Center*, J. Deisenhofer, J.R. Norris, Eds., Academic Press: San Diego, 1993.
5 S. Fukuzumi, Artificial photosynthesis for production of hydrogen peroxide and its fuel cells. *Biochim. Biophys. Acta - Bioenerg.* 2016, **1857**, 604–611.
6 H. Imahori, Y. Mori and Y. Matano, Nanostructured artificial photosynthesis. *J. Photochem. Photobiol. C Photochem. Rev.* 2003, **4**, 51–83.
7 T. Bottari, G. Trukhina, O. Ince and M. Torres, Towards artificial photosynthesis: Supramolecular, donor–acceptor, porphyrin- and phthalocyanine/carbon nanostructure ensembles. *Coord. Chem. Rev.* 2012, **256**, 2453–2477.
8 R. Ciriminna, L. Albanese, F. Meneguzzo and M. Pagliaro, Hydrogen Peroxide: A Key Chemical for Today's Sustainable Development. *ChemSusChem* 2016, **9**, 3374–3381.
9 R. S. Disselkamp, Energy Storage using Aqueous Hydrogen Peroxide. *Energy&Fuels* 2008, **22**, 2771–2774.
10 S. Fukuzumi and Y. Yamada, Hydrogen Peroxide used as a Solar Fuel in One-Compartment Fuel Cells. *ChemElectroChem* 2016, **3**, 1978–1989.
11 G. Goor, J. Glenneberg and S. Jacobi, Hydrogen Peroxide, in *Ullmann's Encyclopedia of Industrial Chemistry*, Wiley-VCH, 2000.
12 G. Irick, Determination of the Photocatalytic Activities of Titanium Dioxides and Other White Pigments. *J. Appl. Polym. Sci.* 1972, **16**, 2387–2395.
13 J. R. Harbour, J. Tromp and M. L. Hair, Photogeneration of hydrogen peroxide in aqueous TiO_2 dispersions. *Can. J. Chem.* 1985, **63**, 204–208.
14 M. C. Markham and K. J. Laidler, A kinetic study of photo-oxidations on the surface of zinc oxide in aqueous suspensions. *J. Phys. Chem.* 1953, **57**, 363–369.
15 T. R. Rubin, J. G. Calvert, G. T. Rankin and W. MacNevin, Photochemical Synthesis of Hydrogen Peroxide at Zinc Oxide Surfaces. *J. Am. Chem. Soc.* 1953, **75**, 2850–2853.
16 A. P. Hong, D. W. Bahnemann and M. R. Hoffmann, Cobalt(II) Tetrasulfophthalocyanine on Titanium Dioxide: A New Efficient Electron Relay for the Photocatalytic Formation and Depletion of Hydrogen Peroxide in Aqueous Suspensions. *J. Phys. Chem.* 1987, **91**, 2109–2117.
17 C. Wang, X. Zhang, B. Yuan, Y. Wang, P. Sun, D. Wang, Y. Wei and Y. Liu, Multi-heterojunction photocatalysts based on WO_3 nanorods: Structural design and optimization for enhanced photocatalytic activity under visible light. *Chem. Eng. J.* 2014, **237**, 29–37.
18 H. Il Kim, O. S. Kwon, S. Kim, W. Choi and J. H. Kim, Harnessing low energy photons (635 nm) for the production of H_2O_2 using upconversion nanohybrid photocatalysts. *Energy Environ. Sci.* 2016, **9**, 1063–1073.
19 K. Ohkubo, K. Suga and S. Fukuzumi, Solvent-free selective photocatalytic oxidation of benzyl alcohol to benzaldehyde by molecular oxygen using 9-phenyl-10-methylacridinium. *Chem. Commun.* 2006, 2018–2020.
20 H. Kotani, K. Ohkubo and S. Fukuzumi, Photocatalytic Oxygenation of Anthracenes and Olefins with Dioxygen via Selective Radical Coupling Using 9-Mesityl-10-methylacridinium Ion as an Effective Electron-Transfer Photocatalyst. *J. Am. Chem. Soc.* 2004, **126**, 15999–16006.
21 H. Kotani, K. Ohkubo and S. Fukuzumi, Formation of hydrogen peroxide from coal tar as hydrogen sources using 9-mesityl-10-methylacridinium ion as an effective photocatalyst. *Appl. Catal. B Environ.* 2008, **77**, 317–324.
22 K. Ohkubo, K. Mizushima, R. Iwata, K. Souma, N. Suzuki and S. Fukuzumi, Simultaneous production of *p*-tolualdehyde and hydrogen peroxide in photocatalytic oxygenation of *p*-xylene and reduction of oxygen with 9-mesityl-10-methylacridinium ion derivatives. *Chem. Commun.* 2010, **46**, 601–603.
23 K. Ohkubo, T. Kobayashi and S. Fukuzumi, Direct Oxygenation of Benzene to Phenol Using Quinolinium Ions as Homogeneous Photocatalysts. *Angew. Chemie - Int. Ed.* 2011, **50**, 8652–8655.
24 K. Ohkubo, T. Kobayashi and S. Fukuzumi, Photocatalytic alkoxylation of benzene with 3-cyano-1-methylquinolinium ion. *Opt. Express* 2012, **20**, A360.
25 K. Ohkubo, A. Fujimoto and S. Fukuzumi, Photocatalytic Monofluorination of Benzene by Fluoride via Photoinduced Electron Transfer with 3‑Cyano-1-methylquinolinium. *J. Phys. Chem. A* 2013, **117**, 10719–10725.
26 Y. Yamada, A. Nomura, T. Miyahigashi and S. Fukuzumi, Photocatalytic production of hydrogen peroxide by two-electron reduction of dioxygen with carbon-neutral oxalate using a 2-phenyl-4-(1-naphthyl)quinolinium ion as a robust photocatalyst. *Chem. Commun.* 2012, **48**, 8329–8331.
27 Y. Yamada, A. Nomura, T. Miyahigashi, K. Ohkubo and S. Fukuzumi, Acetate Induced Enhancement of Photocatalytic Hydrogen Peroxide Production from Oxalic Acid and Dioxygen. *J. Phys. Chem. A* 2013, **117**, 3751–3760.
28 Y. Yamada, A. Nomura, K. Ohkubo, T. Suenobu and S. Fukuzumi, The long-lived electron transfer state of the 2-phenyl-4-(1-naphthyl)quinolinium ion incorporated into nanosized mesoporous silica–alumina acting as a robust photocatalyst in water. *Chem. Commun.* 2013, **49**, 5132–5134.
29 G. Xu, Y. Liang and F. Chen, Continuously photocatalytic production of H_2O_2 with high concentrations using 2-ethylanthraquinone as photocatalyst. *J. Mol. Catal. A Chem.* 2016, **420**, 66–72.
30 H. Görner, Photoinduced oxygen uptake for 9,10-anthraquinone in air-saturated aqueous acetonitrile in the presence of formate, alcohols, ascorbic acid or amines. *Photochem. Photobiol. Sci.* 2006, **5**, 1052–1058.
31 A. F. Khlebnikov, M. V. Golovkina, M. S. Novikov and D. S. Yufit, A Novel Strategy for the Synthesis of 3-(*N*-Heteryl)pyrrole Derivatives. *Org. Lett.* 2012, **14**, 3768–3771.
32 L. D. Funt, M. S. Novikov, G. L. Starova and A. F. Khlebnikov, Synthesis and properties of new heterocyclic betaines: 4-Aryl-5-(methoxycarbonyl)-2-oxo-3-(pyridin-1-ium-1-yl)-2,3-dihydro-1H-pyrrol-3-ides. *Tetrahedron* 2018, **74**, 2466–2474.
33 R. M. Sellers, Spectrophotometric Determination of Hydrogen Peroxide Using Potassium Titanium(IV) Oxalate. *Analyst* 1980, **105**, 950–954.
34 S. B. Brown, P. Jones and A. Suggett, Iron(lll) complex interference in the iodometric determination of hydrogen peroxide. *Anal. Chim. Acta* 1968, **43**, 343–346.
35 J. Nasielski and E. Vander Donckt, Propriété physico-chimiques de composés à caractère aromatique IX. Mise en évidence de complexes de transfert de charge entre des dérivés *N*-méthylés monoaza-aromatiques et des hydrocarbures aromatiques. *Theor. Chim. Acta*, 1964, **2**, 22–28.
36 J. P. Dinnocenzo, P. B. Merkel and S. Farid, Cationic (charge shift) exciplexes. *J. Phys. Chem. A* 2017, **121**, 7903−7909.
K. Ohkubo, S. Fukuzumi and D. A. Nicewicz, 9-Mesityl-10-methylacridinium Perchlorate, in *Encyclopedia of Reagents for Organic Synthesis*, John Wiley&Sons, 2001.

View Article Online
DOI: 10.1039/C9PP00206E

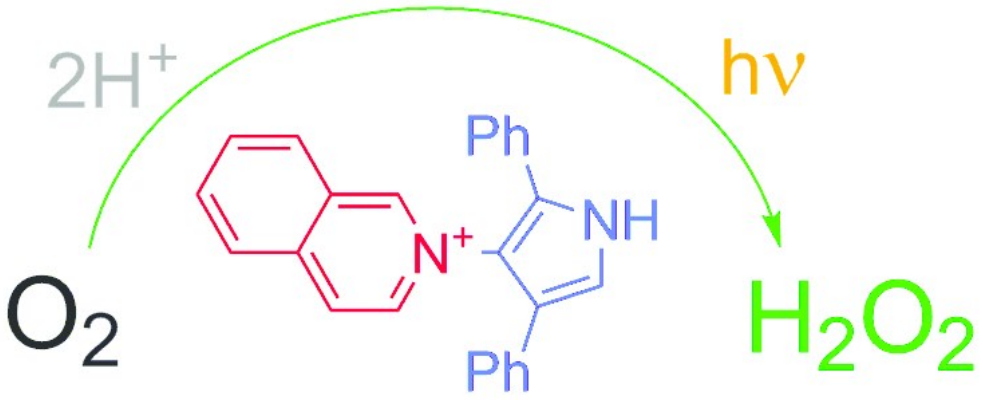

Novel pyrrolo-isoquinoline dyad was shown to be a promissing photocatalyst for O_2 to H_2O_2 reduction using oxalate as a sacrificial electron donor